Journal of Zhejiang University SCIENCE A
ISSN 0000-0000 (Print); ISSN 0000-0000 (Online)
www.zju.edu.cn/jzus; www.springerlink.com
E-mail: jzus@zju.edu.cn

Screening of plane S waves by an array of rigid piles in poroelastic soil*

Yuan-qiang CAI†[1,2], Guang-ya DING†‡[1], Chang-jie XU[1]

([1]*MOE Key Laboratory of Soft Soils and Geoenvironmental Engineering, Zhejiang University, Hangzhou 310027, China*)

([2]*College of Architecture and Civil Engineering, Wenzhou University, Wenzhou 325035, China*)

†E-mail: caiyq@zju.edu.cn; gyding321@yahoo.com.cn

Received Sept. 18, 2007; revision accepted Feb. 26, 2008; published online Mar. 20, 2008

Abstract: An array of rigid piles used as a screening barrier for plane shear (S) waves is investigated in a homogeneous unbounded space. The dynamic poroelastic theory of Biot is employed, under the assumption of an incompressible solid grain. Using Fourier-Bessel series, the problem of multiple scattering is solved by imposing continuity conditions and equilibrium conditions at the soil-pile interfaces with the translational addition theorem. A parametric analysis is conducted to investigate the influence of the permeability of poroelastic soil, separation between piles, number of piles and frequency of incident waves on screening effectiveness of the barrier, and the results are compared with those in an elastic soil medium. Computed results show that the intrinsic permeability of the soil medium displays an apparent effect on the screening of plane S waves.

Key words: Array of rigid piles, Poroelastic soil, Theory of Biot, Scattering, Screening effectiveness
doi:10.1631/jzus.A071494 **Document code:** A **CLC number:** TU4; P315

INTRODUCTION

Vibration sources such as machine foundations, traffic or blasting generate waves that propagate through the ground. These include the Rayleigh wave as well as compressional and shear waves. The energy transmitted by these waves may result in ground amplitudes that cause disturbances to adjacent structures and distress to people. It may be possible to prevent the adverse effects of vibrations on surroundings by providing suitable wave barriers between the source and the structure to be protected.

Traditionally, the solution to the problem is to introduce an open or in-filled trench which can impede the transmission of vibrations in the soil. A recent summary of the relevant literature can be found in (Gao *et al*., 2006). Numerical treatments appeared very recently in literature, include finite element analyses (Yang and Hung, 1997; Shrivastava and Kameswara Rao, 2002; El Naggar and Chehab, 2005); boundary element analyses (Klein *et al*., 1997; Kattis *et al*., 1999a; Al-Hussaini and Ahmad, 2000); and a time domain coupled boundary element-finite element algorithm (Adam and von Estorff, 2005).

In the case of larger wave lengths, the requirements of trench depth often restrict its practical application particularly in very soft ground or high water table level locations. Rows of closely installed piles may be a suitable choice in such cases, which are not limited in terms of depth. The use of piles as wave barriers was proposed by Richart *et al*.(1970). Subsequently, Woods *et al*.(1974) and Liao and Sangrey (1978) experimentally investigated the problem of the screening effectiveness of piles and provided some design guidelines. Aviles and Sanchez-Sesma (1983; 1988) studied the scattering problem by an array of infinite long piles in an elastic medium under various types of incident waves. Boroomand and Kaynia

‡ Corresponding author
* Project (No. 50778136) supported by the National Natural Science Foundation of China

(1991) proposed an approximate analytical mode for studying the screening effectiveness of rigid and elastic piles in the half-space. Kattis *et al*.(1999b) analyzed the problem of vibration isolation with a row of piles in a 3D context by an advanced frequency domain boundary element method (BEM). Kani and Hayakawa (2003) analyzed the effectiveness of PC-wall piles as wave barriers in reducing ground vibrations using field tests and finite element methods (FEMs). Hildebrand (2003) developed an analytical model for evaluating the vibration isolation of a hard wave barrier (e.g. in-filled trench, screen piles, etc.) by using some physically motivated simplifications. Based on the integral equation of Rayleigh wave scattering, Li *et al*.(2005) and Gao *et al*.(2006) presented 3D multi-row piles as ground barriers for passive isolating vibration in a far field. Xu *et al*.(2007a; 2007b) obtained a theoretical solution of scattering coefficients for incident plane compressional and shear waves by the barrier of a row of piles, and studied the trends of the normalized displacements at different places behind the barrier with different types of barriers according to the theoretical solution. Tsai *et al*.(2007) applied a 3D BEM in the frequency domain to investigate the screening effectiveness of circular piles in a row for a massless square foundation subjected to harmonic vertical loading. It is noted that the preceding review has focused primarily on the research work involving homogeneities in single phase media. However, many geophysical applications require a more general model of the environment. Obviously, the single phase model is not appropriate for vibration isolation in practical poroelastic soil. The main drawback of the single phase model is that it cannot predict the influence of the permeability of poroelastic soil on the dynamic response of piles. In such situations it becomes necessary to investigate the screening of plane waves by an array of piles in poroelastic soil.

This paper studies the screening effectiveness of an array of rigid piles for plane shear (S) waves in poroelastic soil. It is assumed that the piles have a circular cross section and are embedded in a homogeneous unbounded poroelastic soil. Furthermore, the piles are assumed to be horizontal in order to retain a usual convention in elastodynamics. Using Fourier-Bessel series and Graf's addition theorem, closed-form solutions are derived for the multiple scattering problem by imposing continuity conditions and equilibrium conditions at the soil-pile interfaces. Finally we consider numerical results for the screening of plane S waves by an array of rigid piles.

GOVERNING EQUATIONS FOR POROELASTIC SOIL

Based on Biot's dynamic theory, the coupled equations that govern the motion of a poroelastic medium can be written as (Biot, 1956)

$$\mu\nabla^2\boldsymbol{U}+(\lambda_c+\mu)\mathrm{grad}e-\alpha M\,\mathrm{grad}\xi=\rho\ddot{\boldsymbol{U}}+\rho_f\ddot{\boldsymbol{w}}, \tag{1}$$

$$\alpha M\,\mathrm{grad}e-M\,\mathrm{grad}\xi=\rho_f\ddot{\boldsymbol{U}}+h\ddot{\boldsymbol{w}}+b\dot{\boldsymbol{w}}. \tag{2}$$

In Eqs.(1) and (2), $\boldsymbol{U}$ and $\boldsymbol{w}$ are the displacement vectors of the solid and fluid relative to the solid, respectively; $\lambda_c=\lambda+\alpha^2M$, where α and M are Biot's parameters accounting for compressibility of the poroelastic material; λ and μ are the Lame's constants; $e=\mathrm{div}\boldsymbol{U}$ and $\xi=-\mathrm{div}\boldsymbol{w}$ are the dilatations of the solid and fluid relative to the solid, respectively; $\rho=(1-f)\rho_s+f\rho_f$, where f is the porosity, ρ_s and ρ_f are the actual mass densities of the solid and the fluid, respectively; $b=\eta/k_s$ is a parameter accounting for the internal friction owing to the relative motion between the solid skeleton and the pore fluid, where η is the fluid viscosity and k_s is the intrinsic permeability of the medium; $h=\rho_f/f$ is a density-like parameter; and overdots denote the derivatives of field variables with respect to time t.

The Helmholtz decomposition theorem allows one to resolve the displacement fields as the superposition of longitudinal and transverse vector components.

$$\boldsymbol{U}=\nabla\varphi+\nabla\psi, \tag{3}$$

$$\boldsymbol{w}=\nabla\chi+\nabla\Theta. \tag{4}$$

where φ and ψ are potentials associated with the solid phase of the bulk material, while potentials χ and Θ are associated with the pore fluid phase.

In the case of steady state, the soil skeleton and fluid displacements are the harmonic function of the angular frequency ω. Thus, omitting the time dependency, and substituting Eqs.(3) and (4) into Boit's

field equations of motion Eqs.(1) and (2), two sets of coupled equations are obtained as

$$\begin{bmatrix} \lambda_c+\alpha^2 M & \alpha M \\ \alpha M & M \end{bmatrix}\begin{bmatrix} \nabla^2\varphi \\ \nabla^2\chi \end{bmatrix}=\begin{bmatrix} -\rho\omega^2 & -\rho_f\omega^2 \\ -\rho_f\omega^2 & -h\omega^2-\mathrm{i}\omega b \end{bmatrix}\begin{bmatrix} \varphi \\ \chi \end{bmatrix}, \tag{5}$$

$$\begin{bmatrix} \mu & 0 \\ 0 & \mu \end{bmatrix}\begin{bmatrix} \nabla^2\psi \\ \nabla^2\Theta \end{bmatrix}=\begin{bmatrix} -\rho\omega^2 & -\rho_f\omega^2 \\ -\rho_f\omega^2 & -h\omega^2-\mathrm{i}\omega b \end{bmatrix}\begin{bmatrix} \psi \\ \Theta \end{bmatrix}, \tag{6}$$

where ∇^2 is the Laplacian operator.

Eqs.(5) and (6) may be manipulated to yield Helmholtz equations:

$$\nabla^2\varphi_{f,s}+p_{1,2}^2\varphi_{f,s}=0,\ \nabla^2\psi+p_3^2\psi=0, \tag{7}$$

where p_1, p_2 and p_3 are the complex wave numbers for the fast compressional wave, slow compressional wave and S wave of the poroelastic medium, defined by

$$p_{1,2}^2=\frac{B\mp\sqrt{B^2-4AC}}{2A},\ p_3^2=\frac{C}{D}, \tag{8}$$

where

$A=(\lambda+2\mu)M$, $B=(\lambda_c+2\mu)(h\omega^2+\mathrm{i}\omega b)+\rho\omega^2 M-2\rho_f\omega^2\alpha M$, $C=\rho\omega^2(h\omega^2+\mathrm{i}\omega b)-\rho_f^2\omega^4$, $D=\mu(h\omega^2+\mathrm{i}b\omega)$.

Employing Eqs.(5)~Eq.(8), with some manipulation, the potentials φ, ψ, χ and Θ can be expressed as

$$\chi=\xi_1\varphi_f+\xi_2\varphi_s,\ \Theta=\xi_3\psi, \tag{9}$$

where the amplitude ratios $\xi_{1,2}$ and ξ_3 are given by

$$\xi_{1,2}=\frac{(\lambda+\alpha^2M+2\mu)p_{1,2}^2-\rho\omega^2}{\rho_f\omega^2-\alpha Mp_{1,2}^2},$$

$$\xi_3=-\frac{\rho_f\omega^2}{h\omega^2+\mathrm{i}b\omega}. \tag{10}$$

SCATTERING OF PLANE S WAVES BY AN ARRAY OF RIGID PILES

Consider plane S waves in a solid matrix with amplitude ψ_0, and incidence angle θ_α, which propagate toward an array of rigid piles as shown in Fig.1. Such incident waves are given in the reference system (x_1, y_1) attached to the first pile by means of

$$\psi^{(i)}(x_1,y_1)=\psi_0\mathrm{e}^{\mathrm{i}p_3(x_1\cos\theta_\alpha+y_1\sin\theta_\alpha)}\cdot\mathrm{e}^{-\mathrm{i}\omega t}. \tag{11}$$

The harmonic problem solution depends on time, t, through the term $\mathrm{e}^{-\mathrm{i}\omega t}$, where ω is the frequency of the incident wave, $\mathrm{i}=\sqrt{-1}$. Thus, all of the resulting parameters depend on this term as well. For the sake of simplicity, this term, $\mathrm{e}^{-\mathrm{i}\omega t}$, will be understood and omitted from now on.

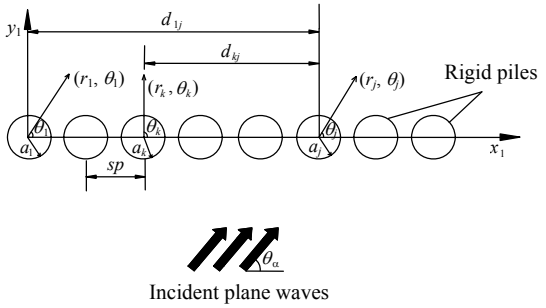

Fig.1 Incident plane S waves and reference systems for each pile

In the presence of an array of rigid piles, the incident waves will be scattered and diffracted around the piles. The solutions are therefore given by

$$\varphi_1=\varphi_f+\varphi_s=\sum_{k=1}^{N}\varphi_f^k(r_k,\theta_k)+\sum_{k=1}^{N}\varphi_s^k(r_k,\theta_k), \tag{12}$$

$$\psi_1=\psi^{(i)}(x_1,y_1)+\psi=\psi^{(i)}(x_1,y_1)+\sum_{k=1}^{N}\psi^k(r_k,\theta_k), \tag{13}$$

where $\varphi_f^k(r_k,\theta_k)$, $\varphi_s^k(r_k,\theta_k)$ and $\psi^k(r_k,\theta_k)$ represent the waves scattered in a solid matrix by the kth pile in terms of the kth system of cylindrical coordinates (r_k, θ_k); N is the number of piles.

Using the method of separation of variables, the scattered field in a solid matrix by the kth pile in the coordinate system (r_k, θ_k) can be written as

$$\varphi_f^k(r_k,\theta_k)=\sum_{n=0}^{\infty}H_n^{(1)}(p_1r_k)(A_{1n}^k\cos n\theta_k+B_{1n}^k\sin n\theta_k),$$

$$\varphi_s^k(r_k,\theta_k)=\sum_{n=0}^{\infty}H_n^{(1)}(p_2r_k)(C_{1n}^k\cos n\theta_k+D_{1n}^k\sin n\theta_k),$$

$$\psi^k(r_k,\theta_k)=\sum_{n=0}^{\infty}H_n^{(1)}(p_3r_k)(E_{1n}^k\sin n\theta_k+F_{1n}^k\cos n\theta_k), \tag{14}$$

where $H_n^{(1)}(\cdot)$ is the Hankel function of the first kind and order n, representing an outgoing wave that satisfies the Sommerfeld's radiation condition at infinity; A_{1n}^k, B_{1n}^k, C_{1n}^k, D_{1n}^k, E_{1n}^k and F_{1n}^k are complex coefficients to be determined from boundary conditions.

In order to formulate the boundary conditions, Eqs.(12) and (13) should be referred to each coordinate system (r_j, θ_j) in which $1\le j\le N$; Eq.(11) can be rewritten in the form

$$\psi^{(i)}(r_1,\theta_1)=\psi_0\cdot\sum_{m=0}^{\infty}\varepsilon_m\mathrm{i}^mJ_m(p_3r_j)\cos[m(\theta_j-\theta_\alpha)]\cdot \mathrm{e}^{\mathrm{i}p_3d_{1j}\cos\theta_\alpha}, \tag{15}$$

where $\varepsilon_0=1$, $\varepsilon_m=2$ when $m\ge1$; $J_m(\cdot)$ is the Bessel function of the first kind and order m; d_{1j} is distance from the origin of system (r_1, θ_1) to the origin of system (r_j, θ_j).

The wave potentials with respect to the cylindrical coordinate systems (r_j, θ_j) and (r_k, θ_k), in which $j\ne k$ are related by the following transformation (Fang, 1995)

$$H_n^{(1)}(p_lr_k)\begin{Bmatrix}\cos n\theta_k\\ \sin n\theta_k\end{Bmatrix}=\frac{1}{2}\sum_{m=0}^{\infty}(-1)^m\varepsilon_mJ_m(p_lr_j)\cdot \begin{Bmatrix}K_m^n(p_ld_{kj})\cos m\theta_j\\ L_m^n(p_ld_{kj})\sin m\theta_j\end{Bmatrix},\ r_j\le d_{kj}, \tag{16}$$

for $j>k$, and

$$H_n^{(1)}(p_lr_k)\begin{Bmatrix}\cos n\theta_k\\ \sin n\theta_k\end{Bmatrix}=\frac{1}{2}(-1)^n\sum_{m=0}^{\infty}\varepsilon_mJ_m(p_lr_j)\cdot \begin{Bmatrix}K_m^n(p_ld_{kj})\cos m\theta_j\\ L_m^n(p_ld_{kj})\sin m\theta_j\end{Bmatrix},\ r_j\le d_{kj}, \tag{17}$$

for $j<k$, where

$$K_m^n(p_ld_{kj})=H_{m+n}^{(1)}(p_ld_{kj})+(-1)^nH_{m-n}^{(1)}(p_ld_{kj}), \tag{18}$$

$$L_m^n(p_ld_{kj})=-H_{m+n}^{(1)}(p_ld_{kj})+(-1)^nH_{m-n}^{(1)}(p_ld_{kj}), \tag{19}$$

where d_{kj} is the distance between the kth pile and the jth pile; l=1, 2, 3.

With the aid of Graf's addition theorem (Fang, 1995), the total wave field in a solid matrix with respect to the cylindrical coordinate system (r_j, θ_j) can be transformed to be expressed in terms of Eqs.(12) and (13):

$$\begin{aligned}\varphi_1=&(1-\delta_{j1})\sum_{k=1}^{j-1}\frac{1}{2}\sum_{n=0}^{\infty}\sum_{m=0}^{\infty}\Big\{(-1)^m\varepsilon_mJ_m(p_1r_j)\Big[A_{1n}^kK_m^n(p_1d_{kj})\cdot\cos m\theta_j+B_{1n}^kL_m^n(p_1d_{kj})\sin m\theta_j\Big]\Big\}+(1-\delta_{jN})\sum_{k=j+1}^{N}\frac{1}{2}\cdot\\ &\sum_{n=0}^{\infty}\sum_{m=0}^{\infty}\Big\{(-1)^n\varepsilon_mJ_m(p_1r_j)\Big[A_{1n}^kK_m^n(p_1d_{kj})\cos m\theta_j+B_{1n}^kL_m^n(p_1d_{kj})\sin m\theta_j\Big]\Big\}+(1-\delta_{j1})\sum_{k=1}^{j-1}\frac{1}{2}\sum_{n=0}^{\infty}\sum_{m=0}^{\infty}\Big\{(-1)^m\cdot\\ &\varepsilon_mJ_m(p_2r_j)\Big[C_{1n}^kK_m^n(p_2d_{kj})\cos m\theta_j+D_{1n}^kL_m^n(p_2d_{kj})\cdot\sin m\theta_j\Big]\Big\}+(1-\delta_{jN})\sum_{k=j+1}^{N}\frac{1}{2}\sum_{n=0}^{\infty}\sum_{m=0}^{\infty}\Big\{(-1)^n\varepsilon_mJ_m(p_2r_j)\cdot\\ &\Big[C_{1n}^kK_m^n(p_2d_{kj})\cos m\theta_j+D_{1n}^kL_m^n(p_2d_{kj})\sin m\theta_j\Big]\Big\}+\\ &\sum_{n=0}^{\infty}H_n^{(1)}(p_1r_j)(A_{1n}^j\cos n\theta_j+B_{1n}^j\sin n\theta_j)+\\ &\sum_{n=0}^{\infty}H_n^{(1)}(p_2r_j)(C_{1n}^j\cos n\theta_j+D_{1n}^j\sin n\theta_j),\end{aligned} \tag{20}$$

$$\begin{aligned}\psi_1=&\psi_0\,\mathrm{e}^{\mathrm{i}p_3d_{1j}\cos\theta_\alpha}\cdot\sum_{m=0}^{\infty}\varepsilon_m\mathrm{i}^mJ_m(p_3r_j)\cos\Big[m(\theta_j-\theta_\alpha)\Big]+\\ &(1-\delta_{j1})\sum_{k=1}^{j-1}\frac{1}{2}\sum_{n=0}^{\infty}\sum_{m=0}^{\infty}\Big\{(-1)^m\varepsilon_mJ_m(p_3r_j)\Big[E_{1n}^kL_m^n(p_3d_{kj})\cdot\sin m\theta_j+F_{1n}^kK_m^n(p_3d_{kj})\cos m\theta_j\Big]\Big\}+(1-\delta_{jN})\sum_{k=j+1}^{N}\frac{1}{2}\cdot\\ &\sum_{n=0}^{\infty}\sum_{m=0}^{\infty}\Big\{(-1)^n\varepsilon_mJ_m(p_3r_j)\Big[E_{1n}^kL_m^n(p_3d_{kj})\sin m\theta_j+F_{1n}^k\cdot K_m^n(p_3d_{kj})\cos m\theta_j\Big]\Big\}+\sum_{n=0}^{\infty}\Big[H_n^{(1)}(p_3r_j)(E_{1n}^j\sin n\theta_j+\\ &F_{1n}^j\cos n\theta_j)\Big].\end{aligned} \tag{21}$$

In the cylindrical coordinate (r_j, θ_j) the radial and tangential displacement components of the skeletal frame and fluid with regard to the solid and the stress components, by using the potentials φ_1, ψ_1, χ_1 and Θ_1, can be derived as

$$u_r=\frac{\partial\varphi_1}{\partial r}+\frac{1}{r}\frac{\partial\psi_1}{\partial\theta},\quad u_\theta=\frac{1}{r}\frac{\partial\varphi_1}{\partial\theta}-\frac{\partial\psi_1}{\partial r},$$

$$w_r=\frac{\partial\chi_1}{\partial r}+\frac{1}{r}\frac{\partial\Theta_1}{\partial\theta},$$

$$\sigma_{rr}=\lambda_c\nabla^2\varphi_1+\alpha M\nabla^2\chi_1+2\mu\left[\frac{\partial^2\varphi_1}{\partial r^2}+\frac{\partial}{\partial r}\left(\frac{1}{r}\frac{\partial\psi_1}{\partial\theta}\right)\right],$$

$$\tau_{r\theta}=\mu\left[2\left(\frac{1}{r}\frac{\partial^2\varphi_1}{\partial r\partial\theta}-\frac{1}{r^2}\frac{\partial\varphi_1}{\partial\theta}\right)+\frac{1}{r^2}\frac{\partial^2\psi_1}{\partial\theta^2}-r\frac{\partial}{\partial r}\left(\frac{1}{r}\frac{\partial\psi_1}{\partial r}\right)\right]. \quad (22)$$

The unknown scattering coefficients A_{1n}^j through F_{1n}^j in Eqs.(20) and (21) must be determined by the application of suitable boundary conditions. At the outer surfaces of each pile, it is assumed that the interfaces are impermeable, the displacements are completely continuous on the interfaces. So the boundary conditions where $r_j=a_j$ can be obtained as

$$u_r^{(i)}(r_j,\theta_j)+u_r^{(s)}(r_j,\theta_j)=X_j\cos\theta_j+Y_j\sin\theta_j, \quad (23)$$

$$u_\theta^{(i)}(r_j,\theta_j)+u_\theta^{(s)}(r_j,\theta_j)=-X_j\sin\theta_j+Y_j\cos\theta_j+r_j\Phi_j, \quad (24)$$

$$w_r^{(i)}(r_j,\theta_j)+w_r^{(s)}(r_j,\theta_j)=0, \quad (25)$$

where $0\le\theta_j\le2\pi$ and j=1,2, …, N; a_j is the radius of the jth pile; X_j and Y_j are rigid body displacements of pile j in the x and y directions, respectively; Φ_j is the rotation of pile j (Fig.2).

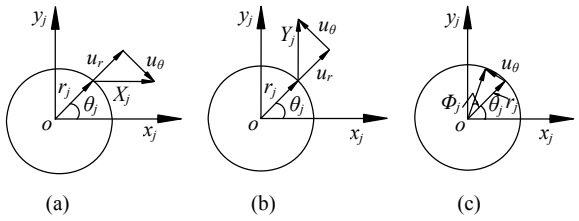

Fig.2 Displacement distribution in each rigid pile. (a) Horizontal translation; (b) Vertical translation; (c) Rotation

From the dynamic equilibrium of pile j, we obtain

$$X_j=-\frac{a_j}{\omega^2M_j}\int_0^{2\pi}(\sigma_{rr}\cos\theta_j-\tau_{r\theta}\sin\theta_j)\Big|_{r_j=a_j}\mathrm{d}\theta_j,$$

$$Y_j=-\frac{a_j}{\omega^2M_j}\int_0^{2\pi}(\sigma_{rr}\sin\theta_j+\tau_{r\theta}\cos\theta_j)\Big|_{r_j=a_j}\mathrm{d}\theta_j,$$

$$\Phi_j=-\frac{a_j^2}{\omega^2J_j}\int_0^{2\pi}\tau_{r\theta}\Big|_{r_j=a_j}\mathrm{d}\theta_j, \quad (26)$$

where M_j denotes the mass of pile j per unit length; J_j denotes the polar moment of inertial of pile j per unit length.

Substituting Eqs.(20) and (21) into Eq.(22), the displacements and stresses at each interface of piles and medium can be obtained. Furthermore, considering the aforementioned transformations, explicit expressions can be obtained for X_j, Y_j and Φ_j, j=1,2, …, N. Then, utilizing the orthogonality of $\cos m\theta_j$ and $\sin m\theta$, and taking into account the linear independence of trigonometric functions, six infinite linear systems of algebraic equations are obtained from Eqs.(23)~(25):

$$\frac{\varepsilon_m}{2}\sum_{n=0}^{\infty}\Bigg[(1-\delta_{j1})\sum_{k=1}^{j-1}(-1)^m A_{1n}^k K_m^n(p_1d_{kj})+(1-\delta_{jN})(-1)^n\cdot\sum_{k=j+1}^{N}A_{1n}^k K_m^n(p_1d_{kj})\Bigg]\cdot(\Lambda_l^{11}+\delta_{m1}R_l^{11})+\frac{\varepsilon_m}{2}\sum_{n=0}^{\infty}\Bigg[(1-\delta_{j1})\cdot\sum_{k=1}^{j-1}(-1)^m C_{1n}^k K_m^n(p_2d_{kj})+(1-\delta_{jN})\sum_{k=j+1}^{N}(-1)^n C_{1n}^k K_m^n(p_2d_{kj})\Bigg]\cdot(\Lambda_l^{12}+\delta_{m1}R_l^{12})+\frac{\varepsilon_m}{2}\sum_{n=0}^{\infty}\Bigg[(1-\delta_{j1})\sum_{k=1}^{j-1}(-1)^m E_{1n}^k L_m^n(p_3d_{kj})+(1-\delta_{jN})\sum_{k=j+1}^{N}(-1)^n E_{1n}^k L_m^n(p_3d_{kj})\Bigg]\cdot(\Lambda_l^{13}+\delta_{m1}R_l^{13})+A_{1m}^j\cdot(\Lambda_l^{14}+\delta_{m1}R_l^{14})+C_{1m}^j\cdot(\Lambda_l^{15}+\delta_{m1}R_l^{15})+E_{1m}^j\cdot(\Lambda_l^{16}+\delta_{m1}R_l^{16})=-\psi_0\,\mathrm{e}^{\mathrm{i}p_3d_{1j}\cos\theta_\alpha}\,\varepsilon_m\mathrm{i}^m\sin m\theta_\alpha\cdot(\Lambda_l^{13}+\delta_{m1}R_l^{13}), \quad (27)$$

$$\frac{\varepsilon_m}{2}\sum_{n=0}^{\infty}\Bigg[(1-\delta_{j1})\sum_{k=1}^{j-1}(-1)^m B_{1n}^k L_m^n(p_1d_{kj})+(1-\delta_{jN})(-1)^n\cdot\sum_{k=j+1}^{N}B_{1n}^k L_m^n(p_1d_{kj})\Bigg]\cdot(\Lambda_l^{21}+\delta_{m1}R_l^{21})+\frac{\varepsilon_m}{2}\sum_{n=0}^{\infty}\Bigg[(1-\delta_{j1})\cdot\sum_{k=1}^{j-1}(-1)^m D_{1n}^k L_m^n(p_2d_{kj})+(1-\delta_{jN})\sum_{k=j+1}^{N}(-1)^n D_{1n}^k L_m^n(p_2d_{kj})\Bigg]\cdot(\Lambda_l^{22}+\delta_{m1}R_l^{22})+\frac{\varepsilon_m}{2}\sum_{n=0}^{\infty}\Bigg[(1-\delta_{j1})\sum_{k=1}^{j-1}(-1)^m F_{1n}^k K_m^n(p_3d_{kj})+(1-\delta_{jN})\sum_{k=j+1}^{N}(-1)^n F_{1n}^k K_m^n(p_3d_{kj})\Bigg]\cdot(\Lambda_l^{23}+\delta_{m1}R_l^{23}+\delta_{m0}S_l^{23})+B_{1m}^j\cdot(\Lambda_l^{24}+\delta_{m1}R_l^{24})+D_{1m}^j\cdot(\Lambda_l^{25}+\delta_{m1}R_l^{25})+F_{1m}^j(\Lambda_l^{26}+\delta_{m1}R_l^{26}+\delta_{m0}S_l^{26})=-\psi_0\,\mathrm{e}^{\mathrm{i}p_3d_{1j}\cos\theta_\alpha}\,\varepsilon_m\mathrm{i}^m\cos m\theta_\alpha(\Lambda_l^{23}+\delta_{m1}R_l^{23}+\delta_{m0}S_l^{23}), \quad (28)$$

where l=1, 2, 3; δ_{m1} and δ_{m0} are the Kronecker deltas; $j=1,2,\cdots,N$; $m=0,1,\cdots,\infty$; $\Lambda_l^{11}\sim\Lambda_l^{26}$, $R_l^{11}\sim R_l^{26}$, S_l^{23} and S_l^{26} are given in Appendix A.

Once the systems of Eqs.(27) and (28) are truncated and solved with an appropriate range for the expansions, the scattering wave field and the total wave field can be obtained. Eq.(22) allows calculation of the displacement fields in each point of the poroelastic soil. The main results will be described later.

NUMERICAL RESULTS

When a time harmonic plane S wave of amplitude ψ_0 propagates normal to the row of piles, the wave is scattered into a combination of fast, slow and shear waves. In addition, for the convenience of numerical calculations, the piles are assumed to be identical and equally spaced with radius a, mass density ρ_2 and separation sp, where sp denotes the distance between the center of adjacent piles, the length of the discontinuous barrier of piles is L, and the origin of the rectangular coordinate system is placed at the center of the barrier (Fig.3). To obtain the numerical results, the following dimensionless material properties and frequency are introduced:

$$\rho_{\mathrm{f}}^*=\rho_{\mathrm{f}}/\rho,\ m^*=h/\rho,\ \lambda^*=\lambda/\mu,\ M^*=M/\mu,$$
$$b^*=\eta d/(k_{\mathrm{s}}\sqrt{\rho\mu}),\ \omega^*=\omega d/C_{\mathrm{s}},\ \rho_2^*=\rho_2/\rho, \quad (29)$$

where d=2a is the diameter of the pile, C_{s} is the S wave velocity in poroelastic soil.

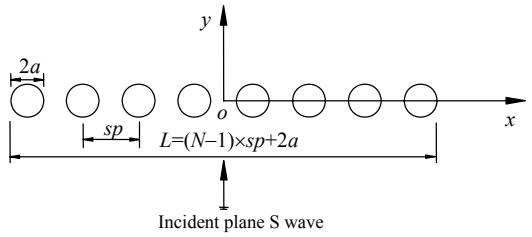

Fig.3 An array of piles and rectangular coordinate system

The properties of soil and pile are presented in Table 1, in which the soil parameters are from (Stoll and Kan, 1981). The normalized displacement amplitude $|u_x/u_0|$ is defined as the ratio of the displacement amplitude of soil behind the barrier to the amplitude of incident plane S waves in the x direction.

Table 1 Dimensionless parameters used in the calculation

Parameter	Value	Parameter	Value
α	1.0	m^*	1.68
λ^*	1.004	b^*	0~500
M^*	246.78	ρ_2^*	1.13
ρ_{f}^*	0.45		

Comparison with existing solutions for ideal elastic soil

As the present study parallels that of Aviles and Sanchez-Sesma (1983) in some cases, we will compare the result of this paper with that obtained by Aviles and Sanchez-Sesma (1983) for an elastic medium. It is noted that if poroelastic parameters M^*, ρ^*, m^*, b^* and α approach zero, then the poroelastic medium is reduced to an elastic medium. Other parameters for calculation are the same as those of Aviles and Sanchez-Sesma (1983). Fig.4 shows the comparison between the present solution and that of Aviles and Sanchez-Sesma (1983), in which $|u_x/u_0|$ designates the ratio of displacement amplitude of soil in the x direction behind the barrier to that of incident S wave, and y/a denotes the dimensionless distance far from the barrier. It can be found that the present solution is in close agreement with that given by Aviles and Sanchez-Sesma (1983).

Influence of internal friction

The influence of internal friction owing to relative motion between the solid skeleton and the pore fluid (b^*) is investigated in Fig.5 with five values of b^* (b^*=0, 5, 50, 100, 500) for x/a=0. Since b^* is inversely proportional to permeability, it means that the material b^*=0 is the most permeable and the material b^*=500 is the least permeable among the five poroelastic materials. The material property b is found to have a more significant influence on the screening effectiveness when compared to other poroelastic material properties. The results shown in Fig.5 clearly indicate that there is a decrease in the normalized displacement amplitudes with increasing values of b^* when y/a>100. It is also observed that the curves for poroelastic soil with b^*=50 and 500 are nearly identical over the entire distance behind the barrier, indi-

cating that when b^* increases to a certain value, the influence of b^* on the screening effectiveness of the barrier can be neglected. All those indicate that, in the case of sand, in which b^* is very small, the coupling effect produced by motions of the solid matrix and the pore fluid is limited. However, in the case of soft clay, in which b^* is large, there is viscous resistance for a flowing fluid in poroelastic soil, which gives rise to the effect of dissipation from the pores of the solid matrix. Consequently, enough flow can occur in clay (high b^*-value) compared to sand (low b^*-value) for viscous losses to become so significant that the results are much better than for an elastic medium.

Influence of number of piles

In the following analyses, the influence of the number of piles on the screening effectiveness is considered, as illustrated in Fig.6. The displacement amplitude of poroelastic soil increases or decrease due to the phase mismatch between the incident and scattering waves after the superposition, which results in the appearance of random values among all curves with y/a<50. It can be seen from Fig.6b, that as the number of piles increases, the optimal screening position is moved backwards, while the normalized displacement amplitude decreases at the places of y/a>180 and the optimal screening region is broadened. At points near the row of piles, the screened zone shows large variability. When the number of piles varies from 6 to 12, the normalized displacement amplitude when y/a=500 changes from 0.79 to 0.61. That is to say, the screening effectiveness of the barrier is improved remarkably. It is also noted from Figs.6a and 6b that the minimum value of the normalized displacement amplitudes are larger at the edge than at the center for the same number of piles, which means that the optimal screening region is at the center of the screened zone.

Comparisons of normalized displacement amplitudes between poroelastic soil and elastic soil

As mentioned previously, most previous

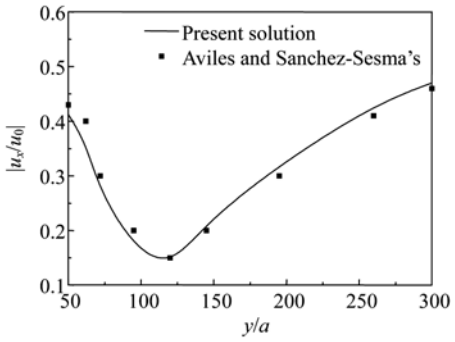

Fig.4 Comparison of normalized displacement amplitudes between the present solution and that of Aviles and Sanchez-Sesma (1983) for elastic soil

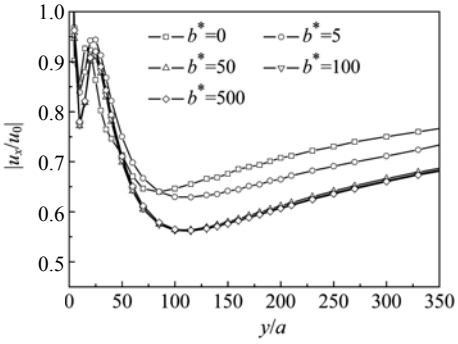

Fig.5 $|u_x/u_0|$ versus y/a with different values of b^* for ω^*=1.0, N=8, sp/a=3, x/a=0

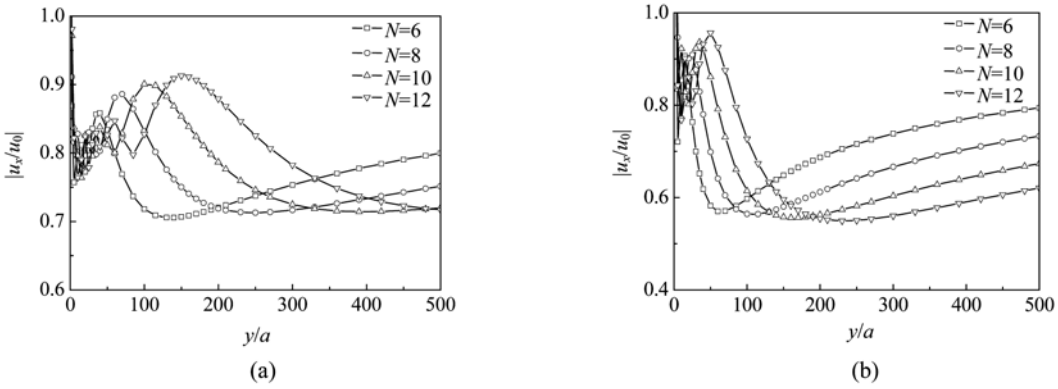

Fig.6 $|u_x/u_0|$ versus y/a with different numbers of piles for ω^*=1.0, sp/a=3, b^*=50. (a) At the edge of screened zone; (b) At the center of screened zone

investigations of the present problem have been limited to an elastic medium. In previous sections, a poroelastic model has been developed for the screening of plane S waves by an array of rigid piles. It is of interest to compare the screening effectiveness of poroelastic soil and elastic soil.

Fig.7 presents a comparison of $|u_x/u_0|$ versus y/a between elastic soil and poroelastic soil with three values of dimensionless frequencies (ω^*=0.5, 1.0, 1.5) for b^*=0 and 500, respectively. It is clear that there is a decrease in the normalized displacement amplitudes as ω^* increases, i.e., the screening effectiveness is improved remarkably with an increase in ω^*. In the case of poroelastic material with b^*=0, the shape of the curves is similar to that of the elastic condition, with only a mild deviation. In the case of poroelastic material with b^*=500, the normalized displacement amplitudes are smaller than that of the elastic condition when y/a>50. Another important conclusion drawn from Fig.7b is that the difference between the normalized displacement amplitudes in poroelastic soil and that in elastic soil increases with increasing ω^*, that is to say, the larger the dimensionless frequency, the better the screening effectiveness in poroelastic soil with b^*=500 than in elastic soil when y/a>100. It is also noted from Fig.7b that the calculated $|u_x/u_0|$ of elastic soil is higher than that of poroelastic soil for all frequencies, due to the fact that there is viscous resistance for a flowing fluid in poroelastic soil, which gives rise to the effect of dissipation from the pores of the solid matrix.

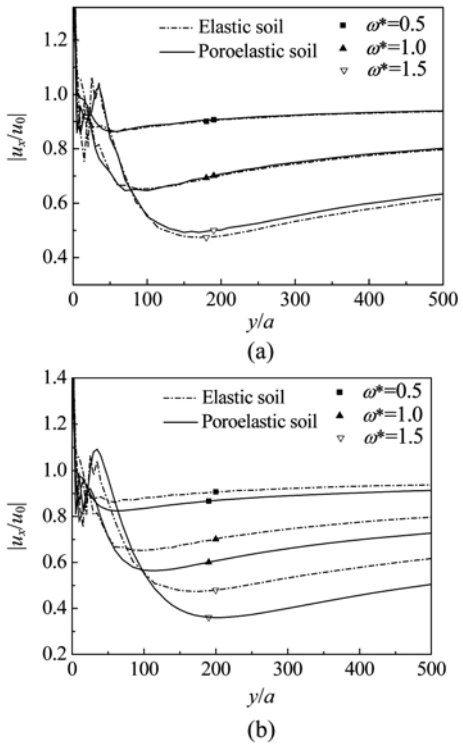

Fig.7 Comparisons of $|u_x/u_0|$ between poroelastic soil and elastic soil with different dimensionless frequencies for N=8, sp/a=3, x/a=0. (a) b^*=0; (b) b^*=500

Fig.8 shows a comparison of $|u_x/u_0|$ versus y/a between elastic soil and poroelastic soil with three values of the separation ratio (sp/a=2.5, 3.0, 3.5) for b^*=0 and 500, respectively. Careful study of these figures reveals that the minimum value of the normalized displacement amplitudes grows with increasing separations. In other words, the larger the separation between piles, the poorer the screening effectiveness of the barrier. Furthermore, some remarkable differences between the curves for elastic soil and poroelastic soil with b^*=500 are observed. This simply means that the screening effectiveness in poroelastic soil with b^*=500 is better than that in elastic soil when y/a>60, while the curves for elastic soil and poroelastic soil with b^*=0 are nearly identical over the entire distance behind the barrier for the same separation. All these results indicate that in the case of sand in which b^* is very small, the shape of the curves is similar to that of the elastic condition, which shows a slight difference in the normalized displacement amplitudes. However, in the case of soft clay in which b^* is large, some significant differences between the normalized displacement amplitudes in poroelastic soil and that in elastic soil can be observed. It is also noted from Fig.8b that the field presents a uniform recovery in the width observed far away from the barrier. That is to say, the pile separation becomes unimportant at large distances behind the barrier. In fact, all of the curves for the poroelastic model come together and tend to attain the level of the incident field in the limit of large y/a. This is due to the fact that the scattering wave field at larger distances becomes weaker, which leads to the infirm interaction between the incident wave field and that of the scattering wave.

Fig.9 gives a comparison of $|u_x/u_0|$ versus y/a between elastic soil and poroelastic soil with three values of the number of piles (N=6, 8, 10) for b^*=0 and 500, respectively. Numerical results presented in Figs.9a and 9b show that, as the number of piles

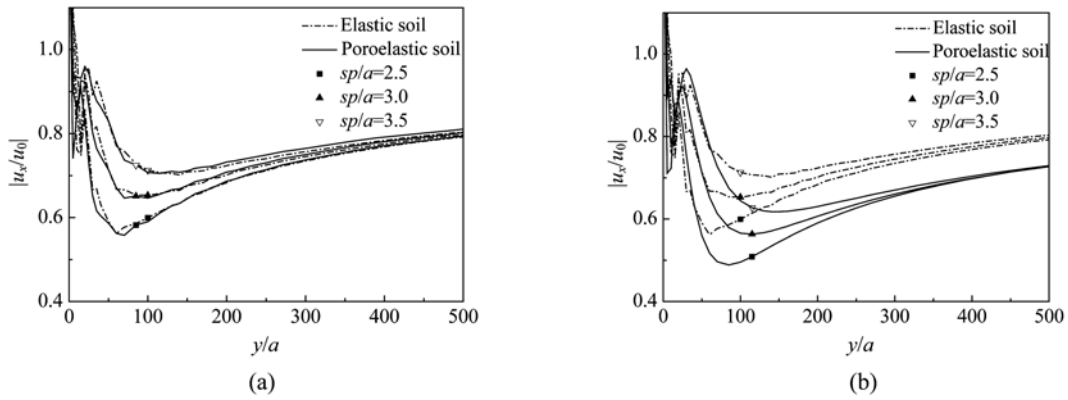

Fig.8 Comparisons of $|u_x/u_0|$ between poroelastic soil and elastic soil with different separations between piles for ω^*=1.0, N=8, x/a=0. (a) b^*=0; (b) b^*=500

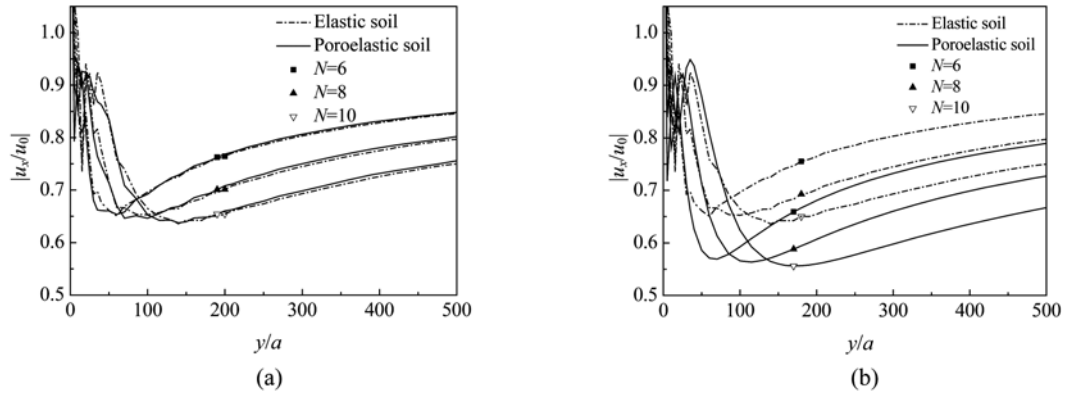

Fig.9 Comparisons of $|u_x/u_0|$ between poroelastic soil and elastic soil with different numbers of piles for ω^*=1.0, sp/a=3, x/a=0. (a) b^*=0; (b) b^*=500

increases, the optimal screening position behind the barrier is moved backwards, and the minimum value of the normalized displacement amplitudes decreases. The curves also show similar trends in elastic soil and in poroelastic soil with b^*=0, while in poroelastic soil with b^*=500, there is a sharp decrease in the normalized displacement amplitudes compared to that in elastic soil when y/a>130.

Figs.5~9 also show an unusual trend for the case of y/a<50, namely, the displacement amplitude of poroelastic soil increases or decreases after the superposition, mainly due to the interaction of incident waves and scattering waves.

CONCLUSION

The presented work demonstrates the need for consideration of the screening of plane S waves by an array of rigid piles in a poroelastic medium. Numerical results show that there is a significant difference in the screening effectiveness of an array of rigid piles between the elastic medium model and the poroelastic medium model. In the case of poroelastic material with b^*=0, the screening effectiveness is similar to that of the elastic condition. However, in the case of poroelastic material with b^*=500, the screening effectiveness is better than that of the elastic condition. All these indicate that some existing methods dealing with the elastic soil medium are adapted to the case in which the intrinsic permeability of the soil is high. Moreover, the screening effectiveness of the barrier is improved as the number of piles increases in poroelastic soil. While the larger the separation between piles, the poorer the screening effectiveness of the barrier in poroelastic soil.

APPENDIX A

$$\Lambda_1^{1l}=-\frac{m}{a_j}J_m(p_la_j)+p_lJ_{m-1}(p_la_j),\ (l=1,2);$$

$$\Lambda_1^{13}=\frac{m}{a_j}J_m(p_3a_j);$$

$$\Lambda_1^{1g}=-\frac{m}{a_j}H_m^{(1)}(p_la_j)+p_lH_{m-1}^{(1)}(p_la_j),\ (l=1,2;\ g=l+3);$$

$$\Lambda_1^{16}=\frac{m}{a_j}H_m^{(1)}(p_3a_j);$$

$$\Lambda_2^{1l}=-\frac{m}{a_j}J_m(p_la_j),\ (l=1,2);$$

$$\Lambda_2^{13}=\frac{m}{a_j}J_m(p_3a_j)-p_3J_{m-1}(p_3a_j);$$

$$\Lambda_2^{1g}=-\frac{m}{a_j}H_m^{(1)}(p_la_j),\ (l=1,2;\ g=l+3);$$

$$\Lambda_2^{16}=\frac{m}{a_j}H_m^{(1)}(p_3a_j)-p_3H_{m-1}^{(1)}(p_3a_j);$$

$$\Lambda_3^{1l}=\xi_l\Lambda_1^{1l},\ (l=1,2,3);$$

$$\Lambda_3^{1g}=\xi_l\Lambda_1^{1g},\ (l=1,2,3;\ g=l+3);$$

$$\Lambda_l^{2g}=\Lambda_l^{1g},\ (l=1,3;\ g=1,2,4,5);$$

$$\Lambda_l^{2g}=-\Lambda_l^{1g},\ (l=1,3;\ g=3,6);$$

$$\Lambda_2^{2g}=-\Lambda_2^{1g},\ (g=1,2,4,5);\ \Lambda_2^{2g}=\Lambda_2^{1g},\ (g=3,6);$$

$$R_1^{1l}=\frac{\lambda_c+\xi_l\alpha M+2\mu}{\rho_2a_j\omega^2}\left[-p_l^2J_1(p_la_j)\right],\ (l=1,2);$$

$$R_1^{13}=-\frac{\mu}{\rho_2a_j\omega^2}p_3^2J_1(p_3a_j);$$

$$R_1^{1g}=\frac{\lambda_c+\xi_l\alpha M+2\mu}{\rho_2a_j\omega^2}\left[-p_l^2H_1^{(1)}(p_la_j)\right],$$

$$(l=1,2;\ g=l+3);$$

$$R_1^{16}=-\frac{\mu}{\rho_2a_j\omega^2}p_3^2H_1^{(1)}(p_3a_j);$$

$$R_2^{1g}=-R_1^{1g},(g=1,2,\cdots,6);$$

$$R_3^{1g}=0,\ R_3^{2g}=0,\ (g=1,2,\cdots,6);$$

$$R_l^{2g}=R_1^{1g},\ (l=1,2;\ g=1,2,4,5);$$

$$R_l^{2g}=-R_1^{1g},\ (l=1,2;\ g=3,6);$$

$$S_1^{23}=S_1^{26}=S_3^{23}=S_3^{26}=0;$$

$$S_2^{23}=\frac{4\mu}{\rho_2a_j\omega^2}\left[-p_3^2J_2(p_3a_j)\right];$$

$$S_2^{26}=\frac{4\mu}{\rho_2a_j\omega^2}\left[-p_3^2H_2^{(1)}(p_3a_j)\right].$$

References

Adam, M., von Estorff, O., 2005. Reduction of train-induced building vibrations by using open and filled trenches. *Computers and Structures*, **83**(1):11-24. [doi:10.1016/j.compstruc.2004.08.010]

Al-Hussaini, T.M., Ahmad, S., 2000. Numerical and Experimental Studies on Vibration Screening by Open and In-Filled Trench Barriers. *In*: Chouw, N., Schmid, G., (Eds.), International Workshop on Wave Propagation, Moving Load and Vibration Reduction (WAVE 2000). Rotterdam Balkema, p.241-250.

Aviles, J., Sanchez-Sesma, F.J., 1983. Piles as barriers for elastic waves. *Journal of Geotechnical Engineering*, **109**(9):1133-1146.

Aviles, J., Sanchez-Sesma, F.J., 1988. Foundation isolation from vibration using piles as barriers. *Journal of Engineering Mechanics*, **114**(11):1854-1870.

Biot, M.A., 1956. Theory of propagation of elastic waves in a fluid-saturated porous solid. I. Low frequency range. *Journal of the Acoustical Society of America*, **28**(2):168-178. [doi:10.1121/1.1908239]

Boroomand, B., Kaynia, A.M., 1991. Vibration Isolation by an Array of Piles. First International Conference on Soil Dynamics and Earthquake Engineering. Karlsruhe, Germany, p.683-691.

El Naggar, M.H., Chehab, A.G., 2005. Vibration barriers for shock-producing equipment. *Canadian Geotechnical Journal*, **42**(1):297-306. [doi:10.1139/T04-067]

Fang, Y.G., 1995. Series solution for scattering of plane SH-waves by multiple shallow circular-arc canyons. *Applied Mathematics and Mechanics* (*English Edition*), **16**(7):657-666.

Gao, G.Y., Li, Z.Y., Qiu, C., Yue, Z.Q., 2006. 3D analysis of rows of piles as passive barriers for ground vibration isolation. *Soil Dynamics and Earthquake Engineering*, **26**(11):1015-1027. [doi:10.1016/j.soildyn.2006.02.005]

Hildebrand, R., 2003. Asymptotic analysis of hard wave barriers in soil. *Soil Dynamics and Earthquake Engineering*, **23**(2):143-158. [doi:10.1016/S0267-7261(02)00154-9]

Kani, Y., Hayakawa, K., 2003. Simulation Analysis about Effects of a PC Wall-pile Barrier on Reducing Ground Vibration. Proceedings of the Thirteenth International Offshore and Polar Engineering Conference. Honolulu, HL, United States, p.1224-1229.

Kattis, S.E., Polyzos, D., Beskos, D.E., 1999a. Modelling of pile wave barriers by effective trenches and their screening effectiveness. *Soil Dynamics and Earthquake Engineering*, **18**(1):1-10. [doi:10.1016/S0267-7261(98)00032-3]

Kattis, S.E., Polyzos, D., Beskos, D.E., 1999b. Vibration isolation by a row of piles using a 3-D frequency domain BEM. *International Journal for Numerical Methods in*

Engineering, **46**(5):713-728. [doi:10.1002/(SICI)1097-0207(19991020)46:5<713::AID-NME693>3.0.CO;2-U]

Klein, R., Antes, H., le Houedec, D., 1997. Efficient 3D modelling of vibration isolation by open trenches. *Computers and Structures*, **64**(1-4):809-817. [doi:10.1016/S0045-7949(96)00418-X]

Li, Z.Y., Gao, G.Y., Qiu, C., Yang, X.J., 2005. Analysis of multi-row of piles as barriers for isolating vibration in far field. *Yanshilixue Yu Gongcheng Xuebao*, **24**(21):3990-3995 (in Chinese).

Liao, S., Sangrey, D.A., 1978. Use of piles as isolation barriers. *Journal of Geotechnical Engineering Division*, *ASCE*, **104**(9): 1139-1152.

Richart, F.E., Hall, J.R., Woods, R.D., 1970. Vibrations of Soils and Foundations. Prentice-Hall, Englewood Cliffs, NJ, p.243-261.

Shrivastava, R.K., Kameswara Rao, N.S.V., 2002. Response of soil media due to impulse loads and isolation using trenches. *Soil Dynamics and Earthquake Engineering*, **22**(8):695-702. [doi:10.1016/S0267-7261(02)00060-X]

Stoll, R.D., Kan, T.K., 1981. Reflection of acoustic waves at a water-sediment interface. *Journal of the Acoustical Society of America*, **70**(1):149-156. [doi:10.1121/1.386692]

Tsai, P.H., Feng, Z.Y., Jen, T.L., 2007. 3D analysis of the screening effectiveness of hollow pile barriers for foundation-induced vertical vibration. *Computers and Geotechnics*, in Press. [doi:10.1016/j.compgeo.2007.05. 010]

Woods, R.D., Barnet, N.E., Sangesser, R., 1974. Holography, a new tool for soil dynamics. *Journal of Geotechnical Engineering Division*, *ASCE*, **100**(11):1231-1247.

Xu, P., Xia, T.D., Zhou, X.M., 2007a. Study on effect of barrier of a row of hollow pipe piles on isolation of incident plane SV waves. *Yantu Gongcheng Xuebao*, **29**(1):131-136 (in Chinese).

Xu, P., Zhou, X.M., Xia, T.D., 2007b. Discontinuous barrier used a row of elastic piles for incident elastic waves. *Zhendong Gongcheng Xuebao*, **20**(4):388-395 (in Chinese).

Yang, Y.B., Hung, H.H., 1997. A parametric study of wave barriers for reduction of train-induced vibrations. *International Journal for Numerical Methods in Engineering*, **40**(20):3729-3747. [doi:10.1002/(SICI)1097-0207(19971030)40:20<3729::AD-NME236>3.0.CO;2-8]